ARTICLE OPEN

Check for updates

Protecting qubit coherence by spectrally engineered driving of the spin environment

Maxime Joos[1], Dolev Bluvstein[1,2], Yuanqi Lyu[1,3], David Weld[1] and Ania Bleszynski Jayich[1]✉

Modern quantum technologies rely crucially on techniques to mitigate quantum decoherence; these techniques can be either passive, achieved for example via materials engineering, or active, typically achieved via pulsed monochromatic driving fields applied to the qubit. Using a solid-state defect spin coupled to a microwave-driven spin bath, we experimentally demonstrate a decoherence mitigation method based on spectral engineering of the environmental noise with a polychromatic drive waveform, and show that it outperforms monochromatic techniques. Results are in agreement with quantitative modeling, and open the path to active decoherence protection using custom-designed waveforms applied to the environment rather than the qubit.

npj Quantum Information (2022)8:47 ; https://doi.org/10.1038/s41534-022-00560-0

INTRODUCTION

Quantum decoherence, resulting from the unavoidable coupling between a qubit and its environment, underlies fundamental descriptions of the quantum-classical transition[1,2] and poses a major challenge to a variety of quantum technologies[3]. Several methods exist to mitigate environment-induced decoherence. Materials-based approaches aim to perfect the environment through techniques like surface passivation and optimized synthesis[4–7]. Dynamical decoupling instead relies on manipulating the qubit rapidly enough to average out deleterious environmental fluctuations at particular frequencies[8–11]. However, the flexibility and power of this technique comes at some cost to the qubit's utility, as the decoupling pulses need to be interleaved with gate operations or sensing sequences[12]. An alternative and complementary approach aims at manipulating the noise frequency spectrum of the bath itself, a technique referred to as spin-bath driving[13] and originally developed in nuclear magnetic resonance and known as spin decoupling[14]. Recent work has shown that monochromatic driving of a spin bath can extend the coherence of bulk[15] and near-surface NV centers[16,17]. An intrinsic limitation of this monochromatic approach is that it does not efficiently address spectrally broad classes of spins that naturally emerge in inhomogeneous environments and interacting spin baths[18].

In this work, we apply a polychromatic drive scheme to a single qubit system and demonstrate experimentally that spectrally engineered driving of a spin bath enhances qubit coherence beyond the limit of what can be achieved with monochromatic driving. The drive is an extension of broad-band decoupling methods[18–22] used in nuclear magnetic resonance and operates in analogy to motional narrowing: driving the spin bath accelerates incoherent bath fluctuations, reducing the integrated phase acquired from the spin bath. Our driving scheme not only enables significantly increased power efficiency for protecting coherence, it also paves the way toward more complex and powerful techniques of tailored dynamical bath engineering.

Figure 1a shows a model of the system we investigate. The polychromatic drive is applied to the spin environment of a shallow nitrogen-vacancy (NV) center in diamond (see Methods for details on the diamond sample preparation). The NV center is a solid-state qubit that exhibits long coherence in ambient conditions and is being used in a variety of applications ranging from networking to quantum sensing. This work uses NV centers located just a few nanometers below the diamond surface, where they are exposed to magnetic noise originating from surface electronic spins[23–27]. The surface character of the spin bath is documented for example in[16,23,26,28] where the coupling to $g = 2$ spins is measured as a function of NV depth, found to be sensitive to surface treatment, and also corroborated by the lack of a $g = 2$ signature for bulk NVs.

Radio-frequency (rf) fields, delivered by a single free-space antenna, enable coherent control of NV qubit states $\{|m_s = 0\rangle, |m_s = -1\rangle\}$ and surface spin qubit states $\{|\uparrow\rangle, |\downarrow\rangle\}$. NV centers are addressed individually by means of a home-built confocal microscope operating in ambient conditions, and are subjected to a static magnetic field $B_0 \approx 315$ G aligned along the NV axis. We use green (532 nm wavelength) laser pulses for initialization and readout of the NV spin state. The NV coherence $C(\tau)$ is probed using the Hahn-echo sequence represented in Fig. 1b; simultaneously, the surface spins are driven with spectrally engineered rf fields. Specifically, we apply drives with Lorentzian spectral line shapes characterized by a tunable full-width at half maximum (FWHM) $\Delta\nu$, generated by stochastic phase modulation of a carrier wave with Rabi frequency Ω_{ss} on the surface spin transition, denoted as a stochastic drive (see Methods for details). Spectrum engineering via phase modulation (as opposed to amplitude modulation) is a key feature of the experiment, ensuring that the driving power remains constant, whereas amplitude modulation could cause fluctuating AC Zeeman shifts of the NV spin states and decohere the NV[16]. The NV coherence time T_2 is extracted from a stretched exponential fit ($\exp[-(\tau/T_2)^n]$) to the measured coherence decay shown in Fig. 1c.

RESULTS

Bath driving

To understand the effect of bath driving on the qubit's coherence, we first give a quantitative description of NV decoherence based

[1]Department of Physics, University of California, Santa Barbara 93106 CA, USA. [2]Department of Physics, Harvard University, Cambridge 02138 MA, USA. [3]Department of Physics, University of California, Berkeley 94720 CA, USA. ✉email: ania@physics.ucsb.edu

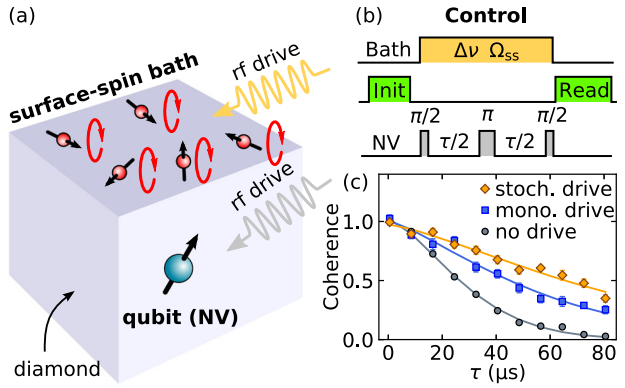

Fig. 1 Coherence extension by driving the spin bath. a A shallow NV center (qubit) is dephased by the magnetic noise originating from a bath of surface spins. **b** Hahn-echo sequence used to measure coherence during bath driving with linewidth $\Delta\nu$ and Rabi frequency Ω_{ss}. **c** Coherence decay without driving (gray), with monochromatic driving (blue) and polychromatic/stochastic driving (orange), described in the text. Solid lines are fits to $\exp[-(\tau/T_2)^n]$. Error bars correspond to ± one standard error of the mean.

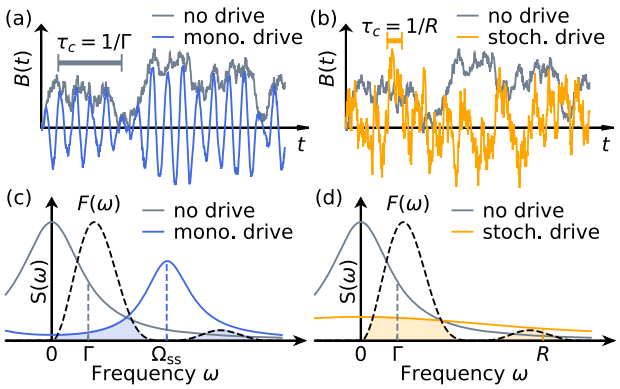

Fig. 2 Principle of monochromatic and stochastic bath driving. Time-domain representations of the magnetic noise $B(t)$ produced by a spin bath, (**a**) for monochromatic driving (blue) and (**b**) for stochastic driving (orange). For simplicity, all the spins are assumed to have the same resonance frequency. Frequency domain representations of the noise spectral density $S(\omega)$, (**c**) for monochromatic driving (blue) and (**d**) for stochastic driving (orange). Both driving methods reduce the overlap between the filter function $F(\tau,\omega)$ (dashed line) and the noise spectrum, as compared to the undriven case (gray curve), resulting in increased coherence.

on a model of the surrounding bath. The NV coherence $C(\tau)$ is determined by the overlap between a filter function and the noise spectral density[29–32]:

$$C(\tau) = \exp\left[-\frac{1}{\pi}\int_0^\infty d\omega S(\omega)F(\tau,\omega)\right], \quad (1)$$

where

$$S(\omega) = \gamma^2 \int_{-\infty}^{\infty} e^{-i\omega t}\langle B(t'+t)B(t')\rangle dt, \quad (2)$$

is the magnetic noise spectral density experienced by the NV (see Fig. 2c, d), γ is the gyromagnetic ratio, B is the field component along the NV axis, $F(\tau,\omega) = 8/\omega^2\sin^4(\omega\tau/4)$ is the qubit Hahn-echo filter function, and ω is the angular frequency. This decoherence model assumes a random Gaussian distribution for the noise amplitudes and is valid in the regime of pure dephasing.

Our strategy to decouple the qubit from its noise environment relies on actively reshaping the spectral density so that it minimally overlaps with the filter function. This decoupling mechanism and its underlying microscopic model are illustrated in Fig. 2. The upper panels are time-domain representations of the magnetic noise $B(t)$ produced by the surface spins, and the lower panels are the corresponding frequency domain representations $S(\omega)$. We now illustrate three cases of driving: no driving, monochromatic, and stochastic.

In the absence of driving (gray curve in Fig. 2), intrinsic spin relaxations at a rate Γ lead to a random process for the noise, characterized by a correlation time $\tau_c = 1/\Gamma$ in the time domain (Fig. 2a, b) and a Lorentzian spectrum with half width at half maximum (HWHM) Γ centered at $\omega = 0$ (Fig. 2c, d). The overlap of the noise spectrum with the Hahn-echo filter function sets the contribution of surface spins to NV decoherence.

In the case of resonant monochromatic bath driving with a Rabi frequency Ω_{ss}, the surface spins undergo Rabi flopping in addition to their intrinsic relaxation dynamics, leading to oscillations of the field $B(t)$ in the time domain (blue curve in Fig. 2a). In the frequency domain (Fig. 2c), monochromatic driving shifts the center of the spectral density from 0 to Ω_{ss}; the overlap with the qubit filter function (represented by the blue shaded area) is consequently reduced from the undriven case.

In contrast, stochastic driving consists of a continuum of frequency tones with random phase relations. Each tone drives partial Rabi oscillations of the surface spins and the incoherent sum of these Rabi oscillations results in random evolution as shown in Fig. 2b). These incoherent dynamics lead to an effective relaxation rate R induced by stochastic driving, on top of the intrinsic relaxation rate Γ (see Supplementary Note 3). In the case of a broad Lorentzian driving spectrum $\Delta\nu \gg \Omega_{ss}, \Gamma$,

$$R = \Gamma + 2\frac{\Omega_{ss}^2}{\Delta\nu}. \quad (3)$$

In the frequency domain (Fig. 2d), the effect of the stochastic drive is to broaden and flatten the noise spectral density. The overlap with the filter function is reduced, leading to an extension of coherence.

In summary, both monochromatic and stochastic driving decouple surface spins by inducing magnetic fluctuations that are fast compared to the Hahn-echo phase sensing time. Compared to monochromatic driving, the advantage of stochastic driving is that it more efficiently addresses the broad spectral range of spins observed in real settings.

Probing bath dynamics under drive

Having discussed the predicted spin dynamics under stochastic excitation and its potential for extending qubit coherence, we now experimentally characterize the frequency and time response of the surface-spin bath and the effects of stochastic driving. We use the NV to probe the surface spins dynamics with the double electron-electron resonance (DEER) sequence shown in Fig. 3a. The Hahn-echo sequence on the NV cancels out low frequency noise from the environment, but the DEER pulse (duration t_{ss}, center frequency f_{ss} and spectral width $\Delta\nu$) selectively recouples the surface spins and reveals their dynamics.

Figure 3b shows the NV coherence as a function of f_{ss}, where the fixed pulse duration $t_{ss} = 60$ ns is chosen to be a π-pulse on resonance with the surface spins. The acquired spectrum exhibits a resonance at (885.3 ± 0.4) MHz which is the magnetic signature of a $g = 2$ spin-1/2 particle in the applied static field of 315 G. The line-shape is best modeled by assuming inhomogeneous broadening of the surface spins and accounting for the finite pulse width t_{ss} (see Supplementary Note 3 for details). From the fit, we extract the FWHM of the underlying Gaussian distribution of the spins $2\Gamma_2 = (15.7 \pm 1.3)$ MHz.

Having confirmed the electronic nature of the surface spins and identified their inhomogeneous broadening, we now investigate the temporal response of the bath. Figure 3c shows the measured

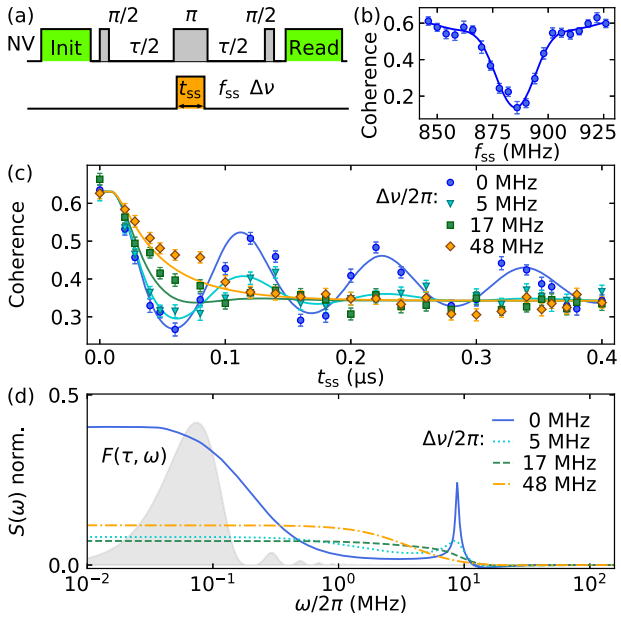

Fig. 3 Probing bath correlations to quantify noise spectrum under drive. a Pulse sequence used to probe the surface spin bath, and (**b**) corresponding spectrum with $\Delta\nu = 0$, $t_{ss} = 60$ ns, $\tau = 20\,\mu$s, $\Omega_{ss}/2\pi = 9.7$ MHz, and an NV π-pulse of 80 ns. **c** Experimental spin bath dynamics, obtained by measuring NV coherence as a function of pulse length t_{ss} for different excitation line-widths $\Delta\nu$ and for $\Omega_{ss}/2\pi = 8.7$ MHz. Increasing $\Delta\nu$ accelerates the damping of the Rabi oscillations, eventually reaching an overdamped regime. **d** Noise spectral densities obtained by Fourier transformation of the fitted DEER signals in (**c**) and normalized so that $2\int_0^\infty S(\omega)d\omega/2\pi = 1$. Gray shaded area represents the Hahn-echo filter function corresponding to a sequence duration of $\tau = 10\,\mu$s. Error bars represent ± one standard error.

NV coherence as a function of t_{ss} for different line-widths $\Delta\nu$ of the drive and a fix sequence duration $\tau = 16\,\mu$s. When $\Delta\nu = 0$, the NV coherence exhibits damped oscillations as a function of t_{ss}. The oscillations reflect the Rabi flopping of the surface spins while the damping is due to the inhomogeneous broadening and the intrinsic relaxation. For $\Delta\nu > 0$, the stochastic DEER pulse decorrelates the field produced by the surface spins between the first and second half of DEER sequence, leading to increased damping of the Rabi oscillations. For $\Delta\nu/2\pi = 48\,\text{MHz} > 2\Gamma_2$, the measured NV coherence decays exponentially at a rate given by Eq. (2), as expected for broad Lorentzian excitation. The solid curves in Fig. 3c are fits using our model of inhomogeneously broadened surface spins subjected to a stochastic drive (see Supplementary Note 3). From these fits, we extract an independent measure of the inhomogeneous broadening $2\Gamma_2 = (14.9 \pm 1.2)$ MHz in agreement with the DEER spectrum in Fig. 3b, and a Rabi frequency $\Omega_{ss}/2\pi = (8.7 \pm 0.1)$ MHz.

To investigate the noise spectrum generated by the measured surface spin dynamics, Fig. 3d shows the Fourier transform of the fitted bath correlations of Fig. 3c obtained after symmetrization with respect to $t_{ss} = 0$. We constrain the integrated power of the spectra to be constant. As expected from the time domain dynamics, the spectrum under monochromatic driving ($\Delta\nu = 0$) exhibits a peak at $\Omega_{ss}/2\pi$, but still has a remaining static component due to the detuned Rabi oscillations of the inhomogeneously broadened spins (the simplified Fig. 2 schematic does not account for this inhomogeneous broadening). In the case of stochastic driving, the noise spectrum is flattened and broadened, and the overlap with $F(\tau, \omega)$ is considerably reduced.

T_2 extension

We now demonstrate that stochastic driving extends NV coherence beyond the gains of monochromatic bath driving. We perform the sequence shown in Fig. 1b and measure the NV coherence time $T_2(\Omega_{SS}, \Delta\nu)$. We observe that stochastic driving outperforms monochromatic driving over a broad range of drive parameters. Figure 4 shows the coherence time $T_2(\Omega_{ss}, \Delta\nu)$, where the bare coherence time $T_2(\Omega_{ss} = 0) = (33.1 \pm 1.5)\,\mu$s. Figure 4a, b highlight the $\Delta\nu$ and Ω_{ss} dependences, respectively. For example, we measure a 2.7-fold increase in coherence time with stochastic driving at ($\Omega_{ss}/2\pi = 4.9$ MHz, $\Delta\nu/2\pi = 17.4$ MHz), as compared to a 1.8-fold increase with monochromatic driving at the same power. Our experimental data are well-captured by Eq. (1) where $S(\omega)$ includes contributions from two g = 2 spin baths (both are driven, but have different bath parameters), and a residual bath that is undriven (see Supplementary Note 3 for details). Details of how the extracted stretch exponent n varies with bath driving parameters are given in Supplementary Note 6.

Our results suggest that, for a given driving power, an optimal $\Delta\nu$ exists that maximizes the coherence. The non-monotonic dependence on $\Delta\nu$ can be understood intuitively as follows: starting from $\Delta\nu = 0$, increasing $\Delta\nu$ enables a larger fraction of the inhomogeneously broadened surface spins to be resonantly addressed and therefore decoupled from the NV center. When $\Delta\nu$ exceeds the inhomogeneous broadening of the surface spins (reported above as $2\Gamma_2 \sim 16$ MHz), drive energy is spread over non-resonant frequencies and the power efficiency of stochastic driving decreases.

Figure 4b also shows that stochastic driving reduces coherence at the lowest Rabi frequencies, an effect also captured by our model. Intuitively, as Ω_{ss} first increases from zero, the noise spectral density broadens, increasing in overlap with the filter function (see Fig. 2d) and decreasing the coherence, before broadening well beyond the peak and flattening out. In Supplementary Note 4, we derive the condition for stochastic driving to increase coherence: $\sqrt{\Gamma R} \gtrsim 2\pi/T_2$. Incorporating two driven baths with long- and short-lived correlations (as suggested by[33]) in our model is essential to quantitatively capture the features of Fig. 4a, b, including the drop of coherence discussed above as detailed in Supplementary Note 4. From the fit in Fig. 4b, we extract the correlation times of the two driven baths: (68 ± 17) μs and $(0.37 \pm 0.05)\,\mu$s.

Finally, we provide a qualitative explanation for the gains of stochastic driving relative to monochromatic driving. In order to completely decouple an ensemble of inhomogeneously broadened spins, monochromatic driving relies on power broadening and requires $\Omega_{ss} \gg \Gamma_2$. On the other hand, stochastic driving naturally addresses all the spins as long as $\Delta\nu \gtrsim \Gamma_2$. Combining this relation with Eq. (2), the condition for decoupling all the spins in the case of stochastic driving is $\Omega_{ss} \gg \sqrt{\Gamma\Gamma_2}$. Therefore, stochastic driving outperforms monochromatic driving as long as $\Gamma < \Gamma_2$, which is often satisfied and, for example, is satisfied by several orders of magnitude for near-surface NV qubits. For the surface spin bath investigated here, we observe $\Gamma_2 \sim 10$ MHz, and expect $\Gamma \sim 0.03$ MHz as reported in[34] (consistent with our observations), explaining the better performance of stochastic driving as $\Gamma \ll \Gamma_2$.

DISCUSSION

A practical advantage of stochastic driving is that it reduces the driving power required to achieve a given coherence extension. AC Zeeman shifts of the qubit energy levels and heating at high rf driving powers are experimental limitations to the coherence time that scale with drive power ($\propto |\Omega_{ss}|^2$)[16]. For example, Fig. 4b shows that doubling the coherence necessitates $\Omega_{ss}/2\pi \approx 3$ MHz for stochastic driving, and ≈8 MHz for monochromatic driving, corresponding to a 7-fold power reduction when stochastic

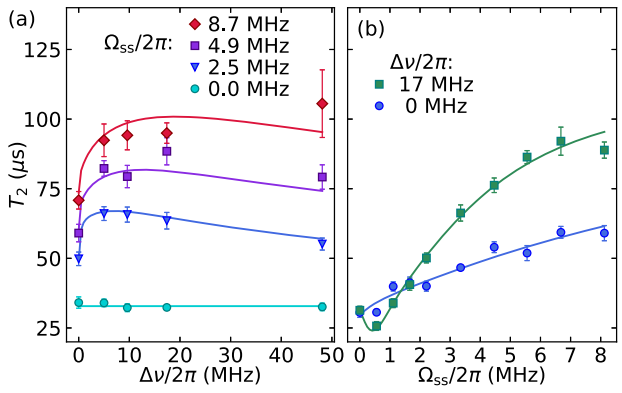

Fig. 4 Coherence time for different driving parameters. a NV T_2 as a function of $\Delta\nu$ for different bath Rabi frequencies Ω_{ss}. Stochastic drive outperforms monochromatic drive ($\Delta\nu = 0$). For very weak driving fields ($\Omega_{ss}/2\pi = 0.0$ MHz), the stochastic phase modulation is ineffective and T_2 is independent of $\Delta\nu$. **b** T_2 as a function of drive Rabi frequency Ω_{ss} for monochromatic driving $\Delta\nu = 0$ and stochastic driving with $\Delta\nu/2\pi = 17$ MHz. Solid lines are fit using our model (see Supplementary Note 3 for details). Error bars correspond to ± one standard deviation of the T2 estimate.

driving is used. This advantage may prove crucial for avoiding heating and other undesired effects, in particular for cryogenic systems like superconducting qubits[35], which could also benefit from spin bath driving techniques. While coherent driving of surface electric dipoles that decohere trapped ion qubits[36–39] or NV qubits[40] may be infeasible, this work suggests that such dipoles could possibly be incoherently driven and motionally narrowed.

In this work, we have considered only driving with a Lorentzian spectrum, but other types of polychromatic driving could be even more advantageous. The drive could for example be engineered to precisely cover the exact spectral shape of the noise sources, and engineering alternative spectral shapes could also enable maximization of the coherence at a desired Rabi frequency. As a proof of concept, we show in Supplementary Note 5 that a Gaussian spectrum for the drive performs better than a Lorentzian spectrum at specific Rabi frequencies. A more complex but potentially also more powerful approach would be to not use any pre-existing knowledge of the noise spectrum, but instead, apply real-time reinforcement learning to converge toward a drive waveform that maximizes the coherence time T_2 of the NV. Ultimately, complex polychromatic waveforms could be used to exploit correlations among bath spins.

In conclusion, we demonstrate the extension of coherence of a qubit by driving its spin environment with spectrally engineered fields. We show that stochastic driving of the surface-spin bath of shallow NV centers is more efficient than monochromatic driving, and corroborate our findings with a quantitative model. Further improvements, especially for mesoscopic baths, may be possible using customized structured drive waveforms. Beyond extending coherence, spectrally engineered driving of the spin environment has much broader applications than merely extending coherence. As an example, recent work has used stochastic driving of an NV center's spin bath to probe the many body dynamics of the bath[41].

METHODS

Diamond sample fabrication

The diamond substrate consists of a commercial Element Six electronic grade (100) diamond plate with dimensions 2 mm × 2mm × 0.15 mm on top of which a 50 nm-thick layer of isotopically purified diamond (99.999% ^{12}C methane precursor gas) is grown by plasma-enhanced chemical vapor deposition. Shallow NV centers are formed by nitrogen-14 implantation (dose = 5.2×10^{10} cm^{-2}, tilt = 7°, energy = 4 keV) followed by high-temperature annealing. The target NV depth is 7 nm. The diamond surface was patterned and etched with O_2 plasma to form nanopillars with diameter 400 nm and height 500 nm, enabling enhanced collection efficiency.

Stochastic drive

For driving surface spins, we use phase modulated rf fields with Lorentzian line shapes centered on the surface spin transition frequency. The modulation scheme is chosen to minimize fluctuations of NV energy levels caused by varying AC Zeeman shifts[16], which would introduce additional dephasing. A driving field with Rabi frequency Ω and detuning $\Delta_{-1} \gg \Omega$ from the $|m_s = 0\rangle \rightarrow |m_s = -1\rangle$ NV transition frequency causes an AC Zeeman shift equal to $\Omega^2/2\Delta_{-1}$. While amplitude modulation causes variations of AC Zeeman shift on the order of Ω^2/Δ_{-1}, phase modulation introduces variations smaller by a factor $\Delta\nu/\Delta_{-1} \sim 0.01$.

Following the phase-diffusion model for lasers[42], we describe the driving field as $\exp[-i(\nu t - \phi(t))]$, where the phase $\phi(t)$ is a stochastic process chosen to produce the desired spectrum. The desired Lorentzian spectrum implies that the wave auto-correlation function has the form of an exponential decay:

$$\left\langle e^{-i\phi(t)} e^{i\phi(t')} \right\rangle = e^{-\frac{\Delta\nu}{2}|t-t'|}. \quad (4)$$

One choice of $\phi(t)$ that satisfies relation (4) is a Gaussian random walk[43], which we use here for generating our stochastic waveforms. The standard deviation σ for the normally distributed steps should follow:

$$\sigma = \sqrt{\Delta\nu\, \delta t}, \quad (5)$$

where δt is the sampling time of the phase trace $\phi(t)$.

Once the random walk $\phi(t)$ is computer generated, the I and Q modulation parameters are given by the real part and imaginary part of $\exp[i\phi(t)]$ respectively.

We use an arbitrary waveform generator (Keysight M8190A) to output the IQ signals and perform phase modulation of a microwave source (Stanford Research Systems, Inc, SG384). For this work, we used a time window of 100 μs and 200,000 samples corresponding to a sampling rate of $1/\delta t = 2$ GHz for the IQ signals. We control the shape and calibrate the bandwidth of the generated rf drives using a spectrum analyzer.

DATA AVAILABILITY

The data that support the findings of this study are available from the corresponding author upon reasonable request.

CODE AVAILABILITY

The codes developed for the numerical simulations are available from the corresponding author upon reasonable request.

Received: 17 September 2021; Accepted: 24 March 2022;
Published online: 29 April 2022

REFERENCES

1. Zurek, W.H. In Quantum Decoherence: Poincaré Seminar 2005, (eds. Duplantier, B. & Raimond, J.-M. & Rivasseau, V.) Ch. 1 (Birkhäuser Basel, 2007).
2. Schlosshauer, M. Quantum decoherence. *Phys. Rep.* **831**, 1–57 (2019).
3. Acín, A. et al. The quantum technologies roadmap: a european community view. *New J. Phys.* **20**, 080201 (2018).
4. Quintana, C. M. et al. Characterization and reduction of microfabrication-induced decoherence in superconducting quantum circuits. *Appl. Phys. Lett.* **105**, 062601 (2014).
5. Kumar, P. et al. Origin and reduction of 1/*f* magnetic flux noise in superconducting devices. *Phys. Rev. Appl.* **6**, 041001 (2016).
6. Ohno, K. et al. Engineering shallow spins in diamond with nitrogen delta-doping. *Appl. Phys. Lett.* **101**, 082413 (2012).
7. Eichhorn, T. R., McLellan, C. A. & Bleszynski Jayich, A. C. Optimizing the formation of depth-confined nitrogen vacancy center spin ensembles in diamond for quantum sensing. *Phys. Rev. Mater.* **3**, 113802 (2019).
8. Viola, L. & Lloyd, S. Dynamical suppression of decoherence in two-state quantum systems. *Phys. Rev. A* **58**, 2733–2744 (1998).

9. Viola, L., Knill, E. & Lloyd, S. Dynamical decoupling of open quantum systems. *Phys. Rev. Lett.* **82**, 2417–2421 (1999).
10. Bylander, J. Noise spectroscopy through dynamical decoupling with a superconducting flux qubit. *Nat. Phys.* **7**, 565–570 (2011).
11. de Lange, G., Wang, Z. H., Ristè, D., Dobrovitski, V. V. & Hanson, R. Universal dynamical decoupling of a single solid-state spin from a spin bath. *Science* **330**, 60–63 (2010).
12. van der Sar, T. Decoherence-protected quantum gates for a hybrid solid-state spin register. *Nature* **484**, 82–86 (2012).
13. Barry, J. F. et al. Sensitivity optimization for NV-diamond magnetometry. *Rev. Mod. Phys.* **92**, 015004 (2020).
14. Slichter, C. P. Principles of Magnetic Resonance (Springer-Verlag Berlin Heidelberg, 1990).
15. Bauch, E. et al. Ultralong dephasing times in solid-state spin ensembles via quantum control. *Phys. Rev. X* **8**, 031025 (2018).
16. Bluvstein, D., Zhang, Z., McLellan, C. A., Williams, N. R. & Jayich, A. C. B. Extending the quantum coherence of a near-surface qubit by coherently driving the paramagnetic surface environment. *Phys. Rev. Lett.* **123**, 146804 (2019).
17. Ishizu, S. et al. Spin coherence and depths of single nitrogen-vacancy centers created by ion implantation into diamond via screening masks. *J. Appl. Phys.* **127**, 244502 (2020).
18. Ernst, R. R. Nuclear magnetic double resonance with an incoherent radio frequency field. *J. Chem. Phys.* **45**, 3845–3861 (1966).
19. Levitt, M. H. & Freeman, R. Composite pulse decoupling. *J. Magn. Reson.* **43**, 502–507 (1981).
20. Levitt, M. H., Freeman, R. & Frenkiel, T. Broadband heteronuclear decoupling. *J. Magn. Reson.* **47**, 328–330 (1982).
21. Basus, V. J., Ellis, P. D., Hill, H. D. W. & Waugh, J. S. Utilization of chirp frequency modulation with 180°-phase modulation for heteronuclear spin decoupling. *J. Magn. Reson.* **35**, 19–37 (1979).
22. Grutzner, J. B. & Santini, R. E. Coherent broad-band decoupling–an alternative to proton noise decoupling in carbon-13 nuclear magnetic resonance spectroscopy. *J. Magn. Reson.* **19**, 173–187 (1975).
23. Mamin, H. J., Sherwood, M. H. & Rugar, D. Detecting external electron spins using nitrogen-vacancy centers. *Phys. Rev. B* **86**, 195422 (2012).
24. Grinolds, M. S. et al. Subnanometre resolution in three-dimensional magnetic resonance imaging of individual dark spins. *Nat. Nanotechnol.* **9**, 279–284 (2014).
25. Myers, B. A. et al. Probing surface noise with depth-calibrated spins in diamond. *Phys. Rev. Lett.* **113**, 027602 (2014).
26. Sangtawesin, S. et al. Origins of diamond surface noise probed by correlating single-spin measurements with surface spectroscopy. *Phys. Rev. X* **9**, 031052 (2019).
27. Stacey, A. et al. Evidence for primal sp2 defects at the diamond surface: Candidates for electron trapping and noise sources. *Adv. Mater. Interf.* **6**, 1801449 (2019).
28. Dwyer, B. L. et al. Probing spin dynamics on diamond surfaces using a single quantum sensor. Preprint at https://arxiv.org/abs/2103.12757 (2021).
29. de Sousa, R. Electron Spin Resonance and Related Phenomena in Low-Dimensional Structures, (eds. Fanciulli, M.) pp. 183–220 (Springer Berlin Heidelberg, 2009).
30. Biercuk, M. J., Doherty, A. C. & Uys, H. Dynamical decoupling sequence construction as a filter-design problem. *J. Phys. B* **44**, 154002 (2011).
31. Degen, C. L., Reinhard, F. & Cappellaro, P. Quantum sensing. *Rev. Mod. Phys.* **89**, 035002 (2017).
32. Cywiński, L., Lutchyn, R. M., Nave, C. P. & Das Sarma, S. How to enhance dephasing time in superconducting qubits. *Phys. Rev. B* **77**, 174509 (2008).
33. Tetienne, J.-P. et al. Spin properties of dense near-surface ensembles of nitrogen-vacancy centers in diamond. *Phys. Rev. B* **97**, 085402 (2018).
34. Sushkov, A. O. et al. Magnetic resonance detection of individual proton spins using quantum reporters. *Phys. Rev. Lett.* **113**, 197601 (2014).
35. Chang, J. B. et al. Improved superconducting qubit coherence using titanium nitride. *Appl. Phys. Lett.* **103**, 012602 (2013).
36. Brownnutt, M., Kumph, M., Rabl, P. & Blatt, R. Ion-trap measurements of electric-field noise near surfaces. *Rev. Mod. Phys.* **87**, 1419–1482 (2015).
37. Daniilidis, N. et al. Fabrication and heating rate study of microscopic surface electrode ion traps. *New J. Phys.* **13**, 013032 (2011).
38. Hite, D. A. et al. Surface science for improved ion traps. *MRS Bull.* **38**, 826–833 (2013).
39. Noel, C. et al. Electric-field noise from thermally activated fluctuators in a surface ion trap. *Phys. Rev. A* **99**, 063427 (2019).
40. Myers, B. A., Ariyaratne, A. & Jayich, A. C. B. Double-quantum spin-relaxation limits to coherence of near-surface nitrogen-vacancy centers. *Phys. Rev. Lett.* **118**, 197201 (2017).
41. Davis, E.J. et al. Probing many-body noise in a strongly interacting two-dimensional dipolar spin system. Preprint at https://arxiv.org/abs/2103.12742 (2021).
42. Eberly, J. H. Atomic relaxation in the presence of intense partially coherent radiation fields. *Phys. Rev. Lett.* **37**, 1387–1390 (1976).
43. Kimble, H. J. & Mandel, L. Resonance fluorescence with excitation of finite bandwidth. *Phys. Rev. A* **15**, 689–699 (1977).

ACKNOWLEDGEMENTS

We thank Shreyas Parthasarathy and Esat Kondakci for careful reading of the manuscript. We gratefully acknowledge support from the US Department of Energy (BES grant No. DE-SC0019241) for surface spin studies and the DARPA DRINQS program (Agreement No. D18AC00014) for driving protocols. We acknowledge the use of shared facilities of the National Science Foundation (NSF) Materials Research Science and Engineering Center (MRSEC) at UC Santa Barbara, DMR 1720256, and the NSF Quantum Foundry through Q-AMASE-i program award DMR-1906325. D.B. acknowledges support from the NSF Graduate Research Fellowship Program (grant DGE1745303) and The Fannie and John Hertz Foundation.

AUTHOR CONTRIBUTIONS

M.J. conducted the experiment and the theoretical analysis. D.B. and A.B.J. proposed the experiment. Y.L. contributed to experiment and theoretical developments. M.J., D.B., D.W., and A.B.J. contributed to data analysis. D.W. and A.B.J. supervised the work.

COMPETING INTERESTS

The authors declare no competing interests.

ADDITIONAL INFORMATION

Supplementary information The online version contains supplementary material available at https://doi.org/10.1038/s41534-022-00560-0.

Correspondence and requests for materials should be addressed to Ania Bleszynski Jayich.

Reprints and permission information is available at http://www.nature.com/reprints

Publisher's note Springer Nature remains neutral with regard to jurisdictional claims in published maps and institutional affiliations.